Electron and Ion Heat Transport with Lower Hybrid Current Drive and Neutral Beam Injection Heating in ASDEX

F.X. Söldner, G.V. Pereverzev, R. Bartiromo, H.U. Fahrbach,
F. Leuterer, H.D. Murmann, A. Stäbler, K.-H. Steuer

IPP 1/271 November 1992

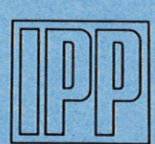

MAX-PLANCK-INSTITUT FÜR PLASMAPHYSIK

8046 GARCHING BEI MÜNCHEN

MAX-PLANCK-INSTITUT FÜR PLASMAPHYSIK
GARCHING BEI MÜNCHEN

Electron and Ion Heat Transport with Lower Hybrid Current Drive and Neutral Beam Injection Heating in ASDEX

F.X. Söldner, G.V. Pereverzev, R. Bartiromo, H.U. Fahrbach,
F. Leuterer, H.D. Murmann, A. Stäbler, K.-H. Steuer

IPP 1/271 November 1992

Die nachstehende Arbeit wurde im Rahmen des Vertrages zwischen dem Max-Planck-Institut für Plasmaphysik und der Europäischen Atomgemeinschaft über die Zusammenarbeit auf dem Gebiete der Plasmaphysik durchgeführt.

ELECTRON AND ION HEAT TRANSPORT WITH LOWER HYBRID CURRENT DRIVE AND NEUTRAL BEAM INJECTION HEATING IN ASDEX *)

F.X. Söldner, G.V. Pereverzev[1], R. Bartiromo[2], H.U. Fahrbach, F. Leuterer, H.D. Murmann, A. Stäbler, K.-H. Steuer

Max-Planck-Institut für Plasmaphysik, D-8046 Garching, Germany, EURATOM Association

[1]I.V.Kurchatov Institute of Atomic Energy, Moscow, Russia, [2]ENEA, Frascati, Italy

Abstract

Transport code calculations were made for experiments with combined operation of Lower Hybrid current drive and heating and neutral beam injection heating on ASDEX. Peaking or flattening of the electron temperature profile is mainly explained with MHD-induced electron heat transport. It is governed by current profile changes due to Lower Hybrid and neutral beam current drive and contributions from the bootstrap current. Ion heat transport can not be described with one single model for all heating scenarios. The ion heat conductivity is reduced during Lower Hybrid heated phases with respect to Ohmic and neutral beam heating and drops below the neoclassical value.

---

*) This report is an extended version of a paper presented at the 19th European Plasma Physics Conference in Innsbruck, Austria, 1992, Vol. II, 961.

1. Introduction

Lower Hybrid current drive (LHCD) and heating were applied together with neutral beam injection (NBI) heating on the ASDEX divertor tokamak. The global energy confinement time shows similar power dependences for the two heating methods /1/. Electrons and ions are heated by NBI, only electrons being heated directly by LH via power input to the suprathermal population. Collisional decoupling of both species in these cases facilitates heat transport studies. A new code recently developed for local transport studies of LHCD plasmas /2/ has been extended to NBI heating and combined operation with LH. In this paper results on electron and ion heat diffusivities with LHCD and NBI combined are presented. The peaking and flattening of the electron temperature profile during LHCD + NBI operation is investigated. Several ion heat transport models were tested in order to reproduce the radial temperature profiles during the different heating scenarios.

2. Transport Code Description

The 1.5D time-dependent transport code ASTRA, originally developed at Kurchatov Institute /3/, is based on a 2D equilibrium solver and 1D transport equations. It was extended for modelling of LH current drive and heating /2/. LH wave propagation is treated with a new approach of diffusive spectrum broadening in k-space in accordance with an analytical solution of the full wave equation /4/. This provides filling of the so-called spectral gap between the launched wave spectrum and the initial thermal electron distribution. The subsequent solution of the kinetic and the wave energy transport equations results in smooth radial LH power deposition and current density profiles similar in shape to those measured in the experiment with the Li beam diagnostics. Multiple bouncing of the wave energy between the plasma interior and edge is applied until full power dissipation. A reflection coefficient R for back-reflection of the wave in the plasma boundary towards the interior was introduced as free parameter. With R = 0.9-0.95 the experimentally measured total power absorption coefficient and its density dependence /5/ are reproduced.

The electron heat conductivity is described by an expression containing four terms with Alcator, anomalous, MHD-enhanced and neoclassical heat conductivity. The anomalous heat conductivity is based on the ITER scaling law for global confinement /6/. This is converted to a local law by replacing the total input power

P_{tot} in the ITER expression by the heating power to the electrons P_e (r) inside a given radius r:

$$\chi_e(r) = C_{Alc}\,\chi_e^{Alc}(r) + C_{ITER}\,\frac{r^2\sqrt{P_e(r)/P_{tot}}}{\tau_E^{ITER}} + C_{MHD}\,\chi_e^{MHD}(r) + \chi_e^{neo}(r) \qquad (1)$$

with

$$\chi_e^{Alc}(r)\ (m^2/s) = \frac{5 \times 10^{19}}{n_e(r)}, \qquad (2)$$

$$\chi_e^{MHD}(r) = (\max(1/q) - 1)\left(1-\left(\frac{r}{2r_s}\right)^2\right)^2 \text{ for } r \le 2r_s, \quad \chi_e^{MHD}(r) = 0 \text{ for } r > 2r_s, \qquad (3)$$

where r_s is the radius of the q = 1 surface (or of the outermost in the case of several q = 1 surfaces).

The neoclassical electron heat conductivity $\chi_e^{neo}(r)$ is taken from Hinton, Hazeltine /7/.

The numerical coefficients in the single terms were adjusted with modelling of one particular LHCD discharge. The sawtoothing OH phase and two LHCD stages, one with m = 1 modes still present, the second with MHD activity fully suppressed, were well described in this discharge. The values $C_{Alc} = 0.18$, $C_{ITER} = 1.5$ and $C_{MHD} = 30$ were obtained for the transport coefficients from these model calculations. They were kept constant in all further calculations. Good agreement between the code calculations and experimental results was then achieved in a wide range of densities and powers for current drive and symmetric wave spectra /2/.

For the modelling of discharges with NBI and combined operation with LH again a validation of the numerical coefficients was carried out. Finally the same model for the electron heat conductivity was retained with the same coefficients as in the previous studies for OH and LH plasmas. The density profiles in these calculations are taken from the experiment. Thomson laser light scattering and HCN laser interferometry are used to determine the electron density. The hydrogen ion dilution is taken into account. The Z_{eff} values are derived from visible bremsstrahlung measurements. A mean ion charge $Z_i = 7$ is assumed, accounting for carbon and oxygen as main impurities according to the spectroscopic measurements. Measured Z_{eff} values are also used in calculating collision frequencies. Collisions with neutral particles are included in the code. The radial profiles of cold and fast

neutrals are treated separately. The beam driven current and the bootstrap current are calculated and taken into account in the radial current density profiles together with Ohmically and LH-driven currents. The beam power deposition profiles were checked independently in calculations with the Monte Carlo code FREYA. A major task finally was the modelling of the ion heat conductivity. Several theoretical and empirical models were tested.

3. Experimental Conditions

All experiments analyzed in this paper were performed on ASDEX in circular double-null divertor plasmas with major radius R = 1.68 m and minor radius a = 0.4 m with deuterium as working gas. The walls of the vacuum vessel were boronized. Neutral hydrogen beams were injected tangentially in the co-direction to the plasma current with an energy E = 52 keV. The absorption coefficient for densities $\overline{n}_e = 1.3 - 3.0 \times 10^{13}$ cm^{-3}, studied here, was in the range 0.7 - 0.8 with about equal partition between ions and electrons. The remaining power is lost through shine-through (5-10 %), orbit losses (5-10%) and charge exchange losses (8-10%). Lower Hybrid waves were injected with low refractive index $\overline{N}_{||} = 2.2$ in directional current drive phasing of the antennae ($\Delta\phi = 90°$ between adjacent waveguides) and in symmetric phasing ($\phi = 0, 0, 90°, 90°,...$). NBI and LH were applied during steady-state flat-top phases of the plasma current and density in sequence with an overlap in between, so that separate stationary phases of each and of combined operation of the two could be analyzed in the same discharge.

4. Electron Heating

Strong central electron heating and peaking of the radial electron temperature profile are obtained with LH-current drive at low density. The profile modification is correlated with the stabilization of the m = 1 mode /8/. With additional heating by NBI into these plasmas, a drop of the central electron temperature and a flattening of the $T_e(r)$ profile are observed in most cases. An example is shown in Fig.1. Neutral beam heating in this discharge is applied with a power $P_{NI} = 1.3$ MW, LHCD with $P_{LH} = 0.94$ MW. Three phases of LH-current drive, combined application of LHCD + NBI and of NBI alone follow in sequence, each with a duration of 0.5 s, long enough to reach steady-state conditions. In Fig.1a the temporal evolution of

the central electron temperature $T_e(0)$ is plotted as obtained from laser light Thomson scattering in the experiment and from the code. After the beginning of the LH pulse $T_e(0)$ rises strongly from 2 keV in the Ohmic phase to 5.8 keV with LH-current drive. The loop voltage drops slightly below zero and the full plasma current is sustained by LHCD. During this phase sawteeth and m = 1 oscillations are suppressed in the experiment /8/. In the calculation the current density profile j(r) broadens, resulting in an increase of q(0) above 1 and the disappearance of the q = 1 surface and the sawtooth inversion radius r_s from the plasma. Both quantities are plotted in Fig.1b. Before q(0) rises above 1, the current profile j(r) becomes first very flat in the central region and then slightly hollow. The inversion radius r_s therefore disappears at finite radius nearly without shrinking.

With the start of NBI, the electron density rises from $\bar{n}_e = 1.3 \times 10^{19}$ m^{-3} during the OH and LH phases to $\bar{n}_e = 2.2 \times 10^{19}$ m^{-3}. The central electron temperature drops to about half-value and saturates slightly above the OH level at 2.7 keV, both in experiment and calculation. The strong rise in density causes the LH-driven current to drop by about 40% in the calculation. The bootstrap current remains small and rises from I_{bs} = 15 kA to I_{bs} = 20 kA. A current I_b = 65 kA with peaked distribution is driven by the beams. The resulting current density profile peaks in relation to LHCD alone. Consequently, q(0) falls below 1 and the inversion radius reappears at the previous position. The subsequent increase of the electron heat conductivity through the MHD-enhanced transport results in degraded electron heating. This sequence consistently explains the drop of $T_e(0)$ in the experiment. There at this time m = 1 modes also reappear. During the whole duration of the NBI phase $T_e(0)$ then stays low as the higher electron density is maintained and m = 1 oscillations continue. All essential features of the behaviour of the electron temperature in the experiment are therefore reproduced by the code.

Similar experiments at higher initial densities $\bar{n}_e = 2.7 \times 10^{19}$ m^{-3} were not affected by a strong rise in density during NBI. An example is given in Fig. 2. Both LH and NBI are injected with the same power P = 1.1 MW. The central electron temperature there rises from $T_e(0)$ = 1.6 keV during the OH phase to 2.8 keV with LH-current drive. It stays on this level with additional NBI heating. After switch-off of the LH it falls back to 1.9 keV with NBI alone. The loop voltage drops from U_l = 1 V during OH to U_l = 0.3 V during LHCD and stays on this level during combined operation of LHCD + NBI. The m = 1 modes in this discharge are stabilized in the experiment for the whole duration of LHCD. In the code calculation the LH-driven current decreases only slightly during additional NBI due to a slight increase in density and

remains at $I_{LH} \approx 250$ kA. The bootstrap current varies between $I_{bs} = 20$ kA during LHCD and NBI phases and $I_{bs} = 25$ kA during combined operation. The beam driven current is smaller than in the low-density discharge discussed above with $I_b = 40$ kA. A broad current profile is then maintained during LHCD and LHCD + NBI combined. The q value stays close to 1 in the central region and the contribution of the MHD term to the electron heat transport therefore remains negligible. The short drop of q(0) after switch-on of NBI causes a brief growth of the MHD-related transport, resulting in a transient drop of $T_e(0)$. This is in remarkable accordance with a small glitch also seen at this instant in the central electron temperature in the experiment. Such transient drops in the central electron temperature were often observed after switch-on of NBI during LHCD. They seem to be caused in general by transient changes in the current distribution, as seen from the transport code calculations.

With symmetric LH wave spectra m = 1 modes are not stabilized in the experiment. Only moderate electron heating is then obtained. Transport code calculations were also performed for this scenario. In this case the current profile is not broadened in the calculations. Therefore the MHD-induced transport is not weakened. In these conditions the increase of the central electron temperature remains small. The electron temperature profile also retains the same shape throughout all phases of the discharge.

The models of electron heat transport and LH power and current deposition developed for LH application to Ohmic target plasmas describe also the various scenarios of combined operation of LH + NBI without further modifications. Changes in the current density distribution by LHCD, NBI-current drive and the bootstrap current can in all cases consistently explain the strong modifications of the electron temperature profile observed in the experiment.

5. Ion Heat Transport

5.1. Reference Discharge

Detailed transport studies were performed for a series of identical discharges with combined operation of LHCD + NBI. Neutral hydrogen beams are injected with a power P_{NI} = 1.8 MW, Lower Hybrid waves in current drive phasing with P_{LH} = 1.1 MW. The temporal evolution of the ion temperature profile in this series was documented by active and passive neutral particle charge exchange analysis. The time behaviour of the loop voltage U_l, the line-averaged density $\bar{n}_e$ and the beta values for the total plasma pressure β_p^{dia} and β_p^{equ} and thermal electron pressure β_p^{el} in a representative discharge (#32988) are shown in Fig. 3. The loop voltage drops to half the Ohmic value during NBI and to zero during LHCD and the phase of LHCD + NBI. The total plasma current is then driven noninductively. The density stays nearly constant at $\bar{n}_e \approx 2.1 \times 10^{13}$ cm^{-3}. Sawteeth are present during NBI and suppressed during LHCD + NBI and during LHCD alone, as seen from the density trace. The difference between equilibrium beta β_p^{equ} and diamagnetic beta β_p^{dia} is due to the beam contribution contained in β_p^{equ} but not in β_p^{dia} during NBI, and due to the suprathermal electrons during LHCD. NBI leads to a strong increase of the total beta values but only a small rise in the electron beta. It therefore results in preferential ion heating. With additional LHCD, both total and electron beta values rise slightly. During the phase with LHCD alone β_p^{el} stays on the same level as during NBI, but the total beta values drop strongly. In this case electron heating then dominates.

5.2. Ion Heat Conductivity Modelling

In the code several models for the ion heat transport were tested with plasma discharge #32988. For these calculations the electron temperature profiles were taken from the experiment. Only the temporal evolution of the ion temperature profile was determined from the transport code in order to single out the ion heat loss channel. Three possible contributions to the ion heat conductivity were investigated: the neoclassical term χ_i^{neo} /9/, a term $\chi_i^{\eta_i}$ due to ion temperature gradient modes (η_i - modes) and drift modes excited by trapped electrons /10/, and a term χ_i^{MHD} connected to MHD activity in the same way as for the electron heat conductivity given in formula (3). The time behaviour of the central ion temperature $T_i(0)$ in the experiment and in the code with the different models is shown in Fig.4.

a) $\chi_i = \chi_i^{neo} + \chi_i^{MHD}$:

With a combination of only neoclassical and MHD-related ion heat transport the Ohmic stage of the discharge is well described. In fact, only neoclassical ion heat conductivity is active in this phase. The MHD-related term χ_i^{MHD} does not affect $T_i(0)$ in the calculations in this phase for two reasons. First, the ion temperature distribution in the plasma centre is flat. Second, the central value q(0) is close to 1 in the Ohmic phase, q(0) = 0.95, and the MHD term, depending on the factor 1 - q(0), is then small. During the Ohmic stage only 0.09 MW (about 25% of the total heating power) is delivered to the ions due to heat exchange with electrons. During the NBI-heated part of the discharge ion heating prevails and about 0.9 MW of the 1.8 MW of net power input is delivered to the ion component. The power input to ions increases by a factor of 10 in comparison with the OH stage. The central ion temperature $T_i(0)$ in the experiment, however, rises only by a factor 2.3, thus indicating strong energy confinement degradation compared with the OH stage. The temperatures calculated in the code are too high in this phase. From the NBI phase to NBI + LHCD the calculated $T_i(0)$ increases further. This originates from the reduction of χ_i^{MHD} due to the j(r) broadening by LHCD. In the central region χ_i^{MHD} is comparable to χ_i^{neo} during NBI. In the stage with LHCD alone the MHD term vanishes completely. The only remaining term of the neoclassical ion heat conductivity gives temperatures in the code still 25% lower than in the experiment. The heat transfer from electrons to ions during LHCD assumes slightly lower values than during the OH stage. The ion temperature, however, is 25% higher during LHCD than in the Ohmic heating phase. This indicates an improvement in ion energy confinement during LHCD.

b) $\chi_i = 2 \times \chi_i^{neo} + \chi_i^{MHD}$:

With a combination of neoclassical ion heat conductivity, with a multiplier of 2, and the MHD-related term, reasonable agreement with the experiment is achieved during OH, NBI and NBI + LHCD. Also no increase of $T_i(0)$ from the NBI stage to NBI + LHCD is obtained in the code, but rather a slight decrease in agreement with the experiment. This is effected by the enhancement of the neoclassical term due to a rise in Z_{eff} from 2.8 during NBI to 3.75 during NBI + LHCD. With the multiplier of 2, the neoclassical term now dominates in this phase over χ_i^{MHD}. During LHCD alone the calculated ion temperatures are again too low.

c) $\chi_i = 2 \times \chi_i^{neo}$:

Code calculations with neoclassical ion heat conductivity alone, with a multiplier of 2, agree with the experiment during OH and NBI + LHCD. They give too high temperatures during NBI and too low temperatures during LHCD. The decrease in $T_i(0)$ from NBI alone to the phase with NBI + LHCD combined is caused by the increase in Z_{eff}. During OH and LHCD the same values as with the combination $\chi_i = 2 \times \chi_i^{neo} + \chi_i^{MHD}$ are obtained, since the MHD term vanishes during these phases.

d) $\chi_i = \chi_i^{neo} + \chi_i^{\eta_i} + \chi_i^{MHD}$:

Instead of an empirical multiplier to the neoclassical ion heat conductivity the anomalous term $\chi_i^{\eta_i}$ based on a theoretical model is introduced to calculate the enhanced losses during the phases with NBI. For the conditions of the discharge considered, the drift mode portion of $\chi_i^{\eta_i}$ of Ref. /10/ is reasonably small and only the η_i mode determines the behaviour of $T_i(0)$. With this combination of all three terms, with multiplier 1 for all, values well below the experimental ones, however, are obtained in the calculations during all phases of additional heating.

The Rebut-Lallia model for ion heat transport /11/ was also tested in modelling. It results, however, in much lower values of $T_i(0)$ in the calculations than in the experiment for all stages of the discharge with additional heating. In the NBI-heated stage the critical electron temperature gradient is exceeded over the external half of the minor plasma radius and for stages with LHCD over the whole plasma cross section. The code then gives very low ion temperatures with $T_i(0) \approx 1.2$ keV during NBI and $T_i(0) \approx 0.3$ keV during NBI + LHCD and during LHCD alone.

A purely empirical ansatz was also tried to model the ion heat conductivity. A link of χ_i at each position to the volume-integrated power inside r as for χ_e with $\chi_i(r) \sim P_i(r)$ gives a wrong radial dependence, because the χ_i profile is usually flat or peaked in the centre. Reasonable agreement with experimental profiles could be obtained in the code by linking χ_i to the local power density with $\chi_i(r) \sim p_i(r)$. With this ansatz it was also possible to reproduce the temporal evolution of the central ion temperature reasonably well.

No model was found which would consistently reproduce the ion temperature profile throughout all phases of additional heating. Already in a previous analysis of NBI-heated plasmas alone with similar parameters the evolution of the ion temperature profile could not be satisfactorily described with one single model for χ_i in all phases /12/. The main problem arises from modelling the LHCD stage. The

ion temperature in this phase is higher than during the Ohmic phase, with smaller power input into the ions. The measured ion temperature profile during LHCD could be reproduced by the code with the simple neoclassical ion heat conductivity, as given in /9/, only by eliminating all additional losses such as MHD transport and charge exchange. Furthermore Z_{eff} has to be reduced from the measured value of 2.5 to nearly 1. But already in Ohmic deuterium discharges at a density $\bar{n}_e = 2 \times 10^{13}$ cm^{-3}, as used in this discharge, values of $Z_{eff} \geq 2$ are usually measured for boronized walls. For the experimental value of Z_{eff} the ion temperature profile during the LHCD phase is fitted with the code only by using for the ion heat conductivity a value a factor 2 below the neoclassical value of ref. /9/

$$\chi_i = 0.5 \times \chi_i^{neo}.$$

5.3. Full Model Calculations

Finally, the different models were also checked with about ten other discharges in the parameter range

$$\bar{n}_e = 1.3 - 3 \times 10^{13}\ cm^{-3},\ I_p = 320 - 420\ kA,\ B_t = 2.2 - 2.8\ T,$$
$$P_{NI} \leq 1.8\ MW,\ P_{LH} \leq 1.2\ MW \text{ (current drive and symmetric wave spectra).}$$

In these cases full model transport code calculations, including the full model for the electron heat conductivity as described above, were performed. Best agreement with measured central ion temperatures was obtained with the combination

$$\chi_i = 2 \times \chi_i^{neo} + \chi_i^{MHD}.$$

The temporal evolution of measured and full model calculated quantities of discharge #32988 is shown in Fig. 5. In the first phase with NBI alone about 1/3 of the plasma current of I_p = 320 kA is driven noninductively with $I_{CD} = I_b + I_{bs}$= 100 kA (Fig. 5a). With additional LHCD, full noninductive current drive is then achieved with the combination of beam-driven, bootstrap and LH-driven currents. This scenario is proposed as first option for ITER /13/. The radial current density profiles during the different phases are plotted in the upper row of Fig. 6. During NBI the j(r) profile peaks with respect to the Ohmic phase due the more peaked beam driven current. Consequently q(0) decreases and the sawtooth inversion radius expands (Fig. 5b).

With the beginning of LHCD j(r) starts broadening and q(0) rises. It approaches 1 during the phase with LHCD alone. The sawtoothing region then shrinks. The progressive flattening of j(r) with LHCD results in a gradual reduction of the MHD-related electron heat transport. This causes in the code calculations an increase of $T_e(0)$ and a peaking of $T_e(r)$ during LHCD, as seen from Fig. 5c. This is in good agreement with the experimental observations. Also the temporal evolution of the volume-averaged electron temperatures in the experiment is well reproduced by the code. Ion heating prevails during NBI alone and the central ion temperature $T_i(0)$ exceeds $T_e(0)$, as seen from Fig. 5d,c. $T_i(0)$ remains on the same level during the subsequent phase of NBI + LHCD combined. With LHCD continuing alone after NBI, $T_i(0)$ drops nearly to the Ohmic level. The large difference between electron and ion temperatures in this phase is explained by the small heat transfer from electrons to ions during pure electron heating from the LH at high electron temperature. The code reproduces the ion temperatures well during the Ohmic, NBI and combined NBI + LHCD phases. For LHCD alone it gives values about a factor 2 too low.

Radial profiles of power input densities to electrons and ions in the code and temperatures and heat conductivities from experiment and code calculation are plotted in Fig. 6 for the three phases of NBI, LHCD + NBI combined and for LHCD alone. The power input to electrons and ions is about equal during NBI and LHCD + NBI. The radial profiles of $p_i(r)$ during these phases are more peaked than $p_e(r)$. During LHCD the power input to the ions in the central region is a factor of more than 20 smaller than during NBI. It is a factor of about 10 smaller than the input to the electrons. The radial profiles of the electron temperatures and heat conductivities calculated with the transport code agree well with the experiment. The electron heat conductivity $\chi_e(r)$ increases towards the plasma edge in all phases. This radial variation is more pronounced during LHCD, when the MHD-related transport affecting the central region is suppressed. The measured $T_i(r)$ profiles during NBI and NBI + LHCD exhibit a shoulder in the peripheral region. This is very likely a systematic overestimate in the charge exchange measurements caused by the presence of fast particles in this region /14/. Apart from this shoulder the ion temperature profiles from experiment and calculations are in reasonable agreement during NBI and NBI + LHCD. During LHCD alone the code gives too low values over the whole profile.

Summary

Electron and ion heat transport were investigated with a 1.5D transport code for heating with LH and NBI into the same target plasmas. The model of electron heat transport originally developed for the analysis of LH heating and current drive of Ohmic target plasmas is also valid for the combined operation of LH + NBI. The high central electron temperatures after m=1 stabilization by LHCD are well reproduced by the code. Peaking and flattening of the electron temperature profile are correlated with variations of the current density profile arising from the different contributions of peaked beam-driven current and broad LH-driven current distributions. The resulting MHD-related transport determines the form of the electron temperature profile. The ion heat transport cannot be represented in the form of a single model for all heating scenarios. The phases with OH, NBI and NBI + LH heating are well described with a combination of twice neoclassical and an MHD-related ion heat conductivity. But a reduction of χ_i below the neoclassical value has to be assumed in order to reproduce with the code the ion temperature profiles in the experiment during LHCD. The contribution of the ion component to the total plasma energy content is small, however, under the conditions of direct electron heating with LH alone studied here. The improved ion energy confinement during LHCD was therefore not discovered in global energy confinement studies.

The Lower Hybrid experiments were performed in collaboration between IPP Garching, ENEA Frascati and PPPL Princeton.

References

/1/ Söldner, F.X., et al., 18th Europ. Conf. on Contr. Fusion and Plasma Physics, Berlin 1991, Vol. III, 405.

/2/ Pereverzev, G.V., et al., Nucl. Fusion 32, 1023 (1992).

/3/ Pereverzev, G.V., et al., Internal report IPP 5/42 (1991), Max-Planck-Institut für Plasmaphysik, Garching, Germany.

/4/ Pereverzev, G.V., Nucl. Fusion 32, 1091 (1992).

/5/ Bartiromo, R., et al., 17th Europ. Conf. on Contr. Fusion and Plasma Physics, Amsterdam 1990, Vol. III, 1092.

/6/ Yushmanov, P.N., et al., Nucl. Fusion 30, 1999 (1990).

/7/ Hinton, F.L., R.D. Hazeltine, Rev. Mod. Phys. 48, 239 (1976).

/8/ Söldner, F.X, et al., 13th Int. Conf. on Plasma Physics and Controlled Nuclear Fusion Research, Washington 1990, Vol. 1, 613.

/9/ Chang, C.S., Hinton, F.L., Phys. Fluids 29, 3314 (1986).

/10/ Romanelli, F., Plasma Physics and Contr. Fusion 31, 1535 (1989).

/11/ Rebut, P.-H., et al., Phys. Fluids B 3, 2209 (1991).

/12/ Stroth, U., et al., 18th Europ. Conf. on Contr. Fusion and Plasma Physics, Berlin 1991, Vol. I, 101.

/13/ ITER documentation series No. 32, IAEA, Vienna (1991).

/14/ Berezovskij, E.L., et al., Nucl. Fusion 27, 2019 (1987).

Figure Captions

Fig.1: Temporal evolution of characteristic parameters in a discharge with LHCD + NBI at low density:
(a) measured and calculated values of the central electron temperature $T_e(0)$,
(b) sawtooth inversion radius r_s and central q-value q(0) in code calculation.
$\bar{n}_e(OH) = 1.3 \times 10^{13}$ cm^{-3}, $B_t = 2.8$ T, $I_p = 420$ kA, $P_{NI} = 1.3$ MW, $P_{LH} = 0.94$ MW, LH in current drive phasing: $\Delta\phi = 90°$, $\bar{N}_{||} = 2.2$.

Fig.2: Temporal evolution of characteristic parameters in a discharge with LHCD + NBI at higher density:
(a) measured and calculated values of the central electron temperature $T_e(0)$,
(b) sawtooth inversion radius r_s and central q-value q(0) in code calculation.
$\bar{n}_e(OH) = 2.7 \times 10^{13}$ cm^{-3}, $B_t = 2.8$ T, $I_p = 420$ kA, $P_{NI} = 1.1$ MW, $P_{LH} = 1.1$ MW, LH in current drive phasing: $\Delta\phi = 90°$, $\bar{N}_{||} = 2.2$.

Fig.3: Temporal evolution of characteristic plasma parameters in a discharge with combined operation of LHCD and NBI:
(a) loop voltage U_l, **(b)** line-averaged density $\bar{n}_e$, **(c)** beta values.
$B_t = 2.2$ T, $I_p = 320$ kA, $P_{NI} = 1.8$ MW, $P_{LH} = 1.1$ MW, LH in current drive phasing: $\Delta\phi = 90°$, $\bar{N}_{||} = 2.2$.

Fig.4: Temporal evolution of the central ion temperature $T_i(0)$ in experiment (#32988) and code calculation with different models for the ion heat conductivity.

Fig.5: Temporal evolution from code calculation:
(a) total noninductively driven current I_{CD} and LH-driven current I_{LH},
(b) sawtooth inversion radius r_s and central q-value q(0),
(c) central and volume averaged electron temperatures $T_e(0)$, $\langle T_e \rangle$,
(d) central ion temperature $T_i(0)$.
Electron and ion temperatures from experiment are added in solid lines in the figure sections **(c)** and **(d)**.

Fig.6: Radial profiles of current densities (j_{tot}= total current, j_{cd}= noninductively driven current), power input to electrons and ions p_e, p_i, electron and ion temperatures T_e, T_i, and electron and ion heat conductivities χ_e, χ_i.

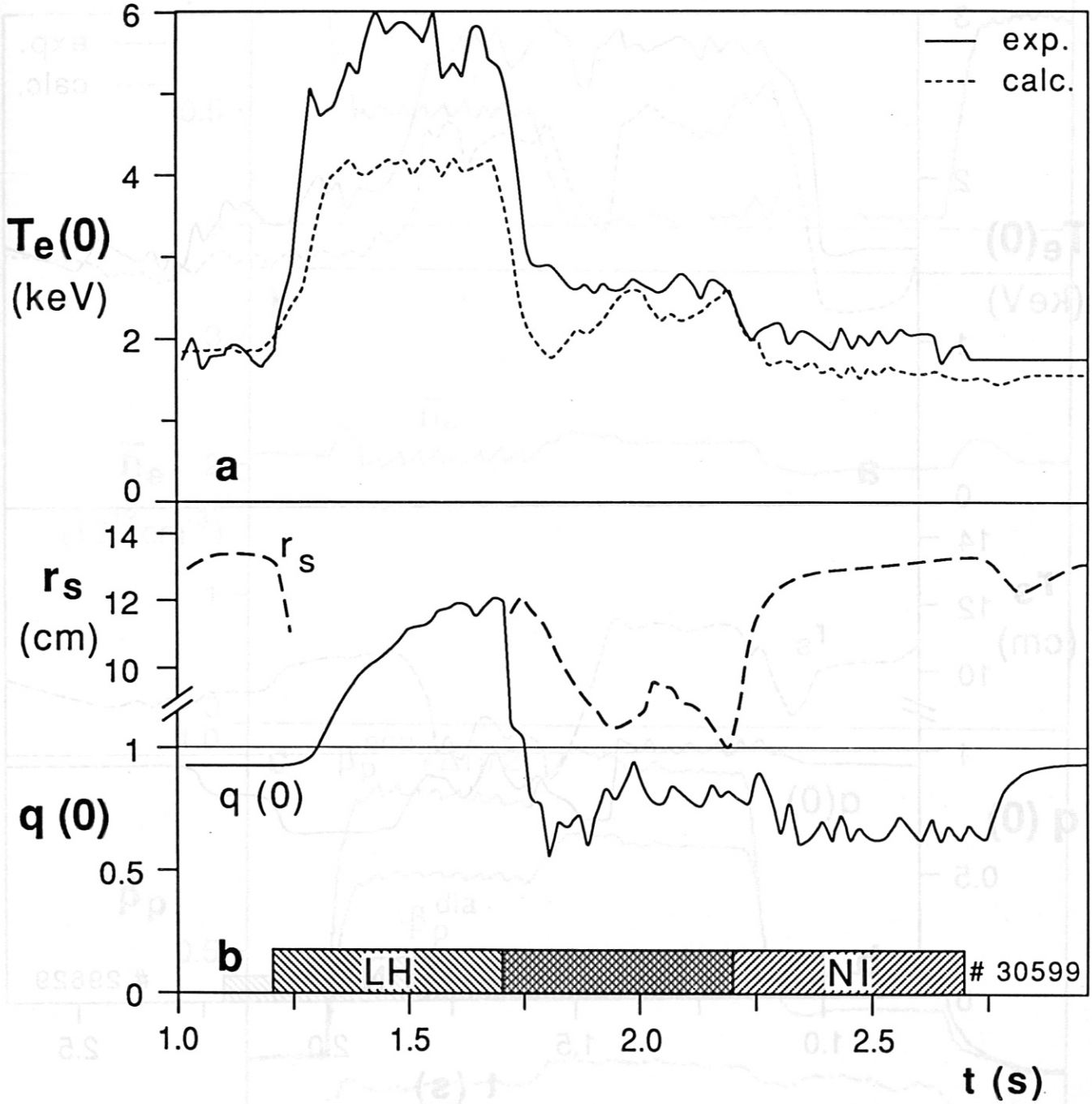
6
4
2
0
exp.
calc.
$T_e(0)$
(keV)
a
14
12
10
1
0.5
0
r_s
(cm)
r_s
q (0)
q (0)
b
LH
NI
30599
1.0
1.5
2.0
2.5
t (s)

Fig. 1

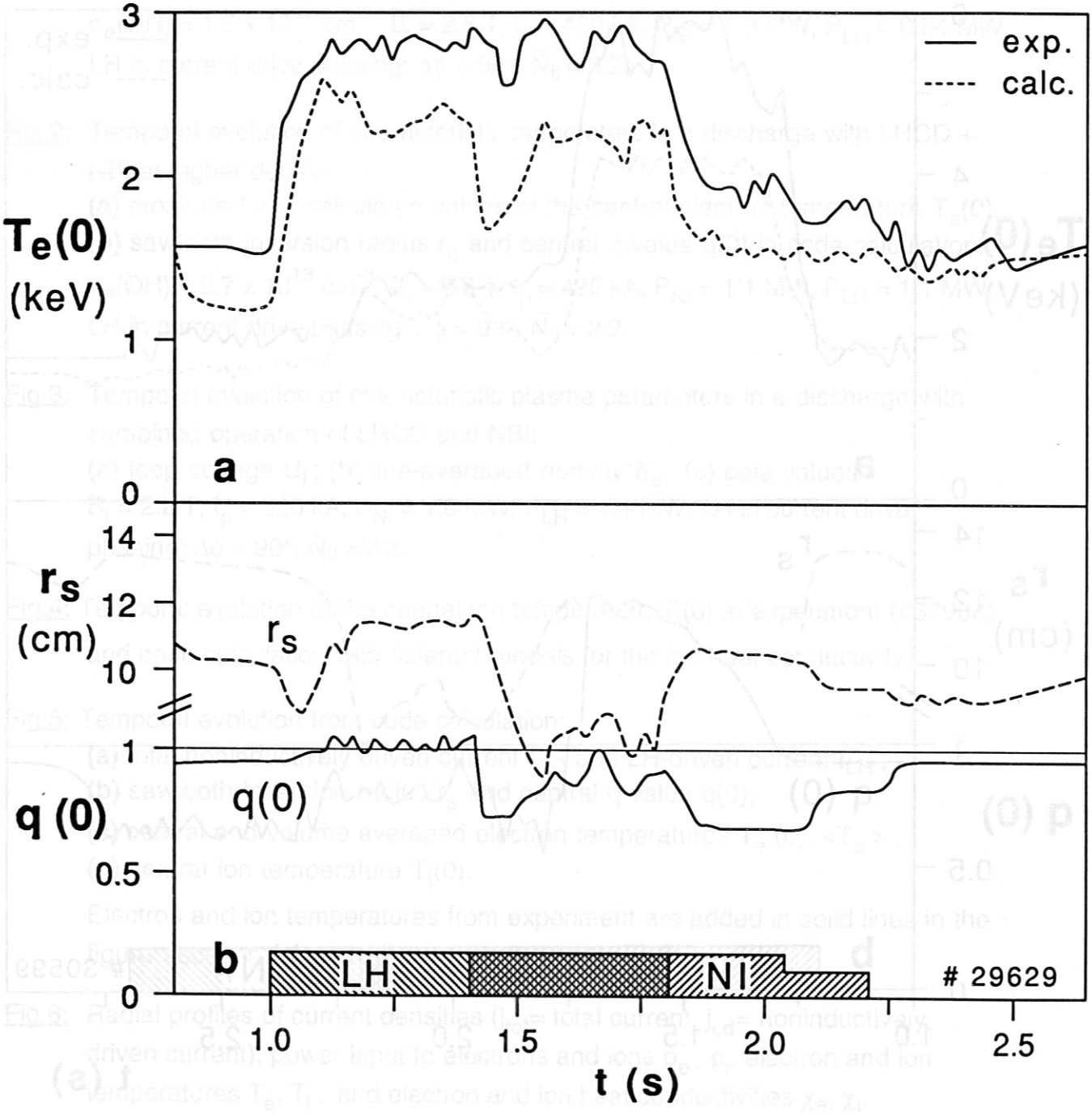
3
2
1
0
$T_e(0)$
(keV)
exp.
calc.
a
14
12
10
1
0.5
0
r_s
(cm)
r_s
q(0)
$q(0)$
b
LH
NI
29629
1.0
1.5
2.0
2.5
t (s)

Fig. 2

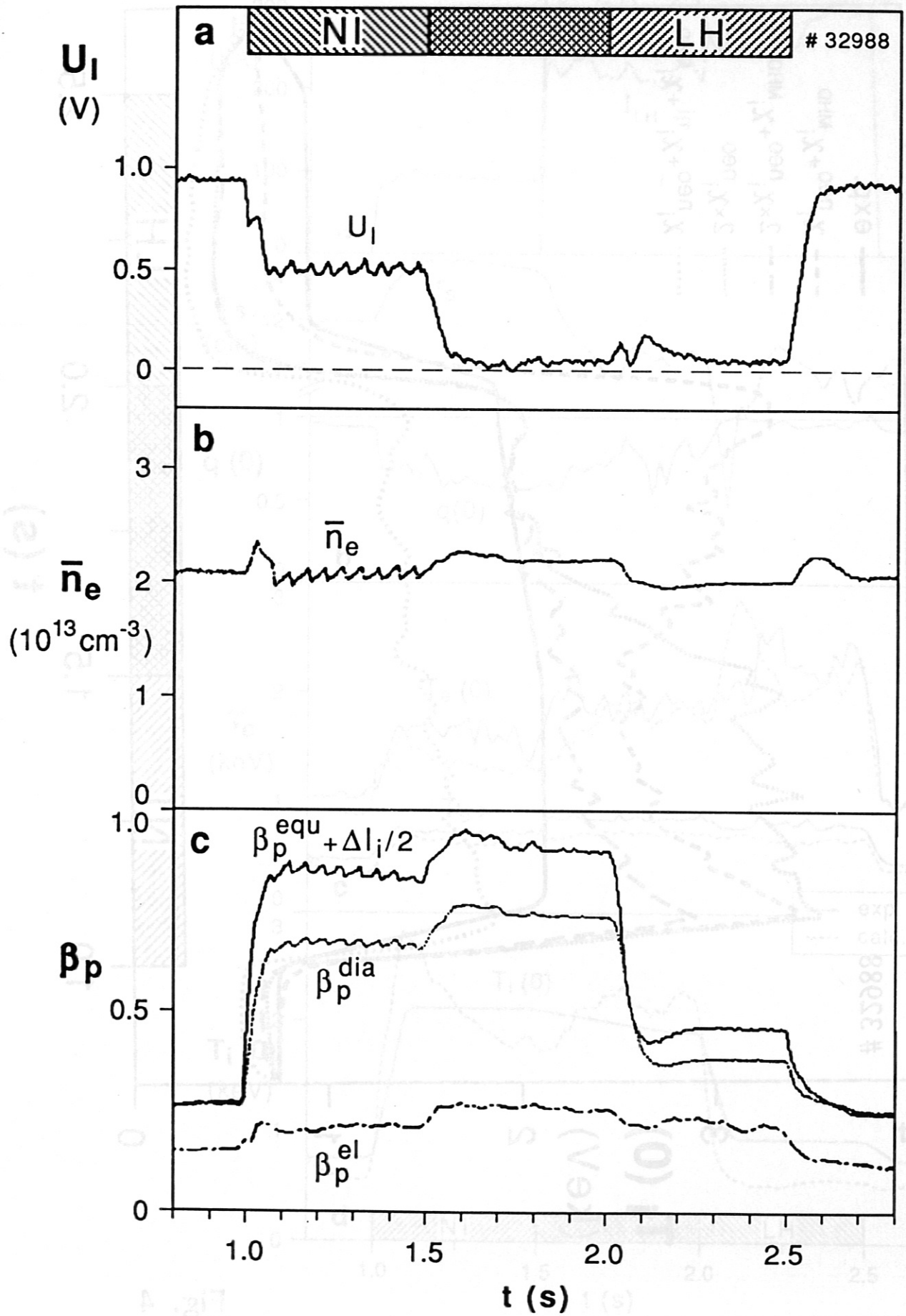
a
NI
LH
32988
U_l
(V)
1.0
0.5
0
U_l
b
3
2
1
0
$\bar{n}_e$
$\bar{n}_e$
$(10^{13}cm^{-3})$
c
1.0
0.5
0
β_p
$\beta_p^{equ}+\Delta l_i/2$
β_p^{dia}
β_p^{el}
1.0
1.5
2.0
2.5
t (s)

Fig. 3

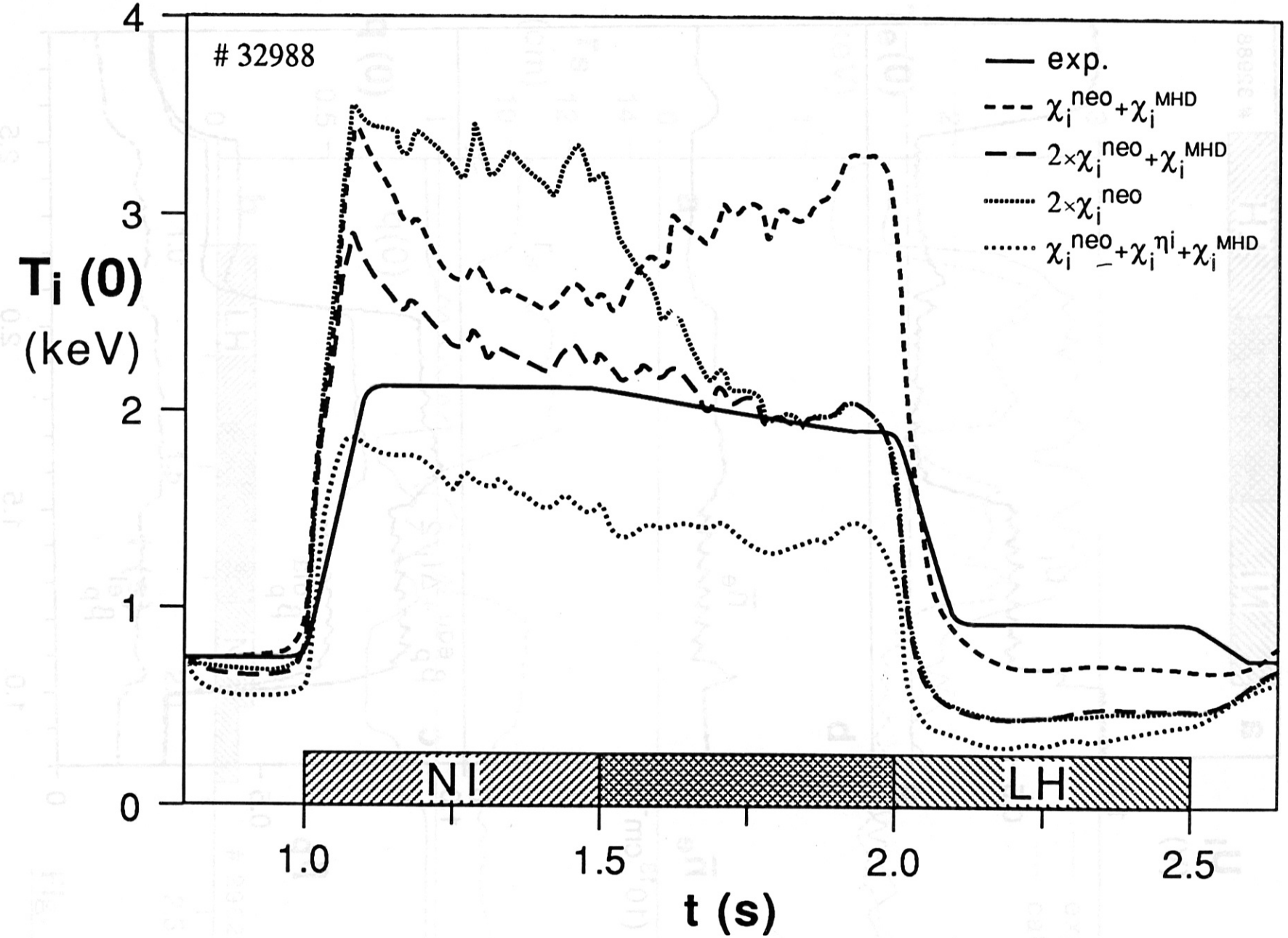
32988
exp.
$\chi_i^{neo}+\chi_i^{MHD}$
$2\times\chi_i^{neo}+\chi_i^{MHD}$
$2\times\chi_i^{neo}$
$\chi_i^{neo}+\chi_i^{\eta i}+\chi_i^{MHD}$
T_i (0)
(keV)
4
3
2
1
0
NI
LH
1.0
1.5
2.0
2.5
t (s)

Fig. 4

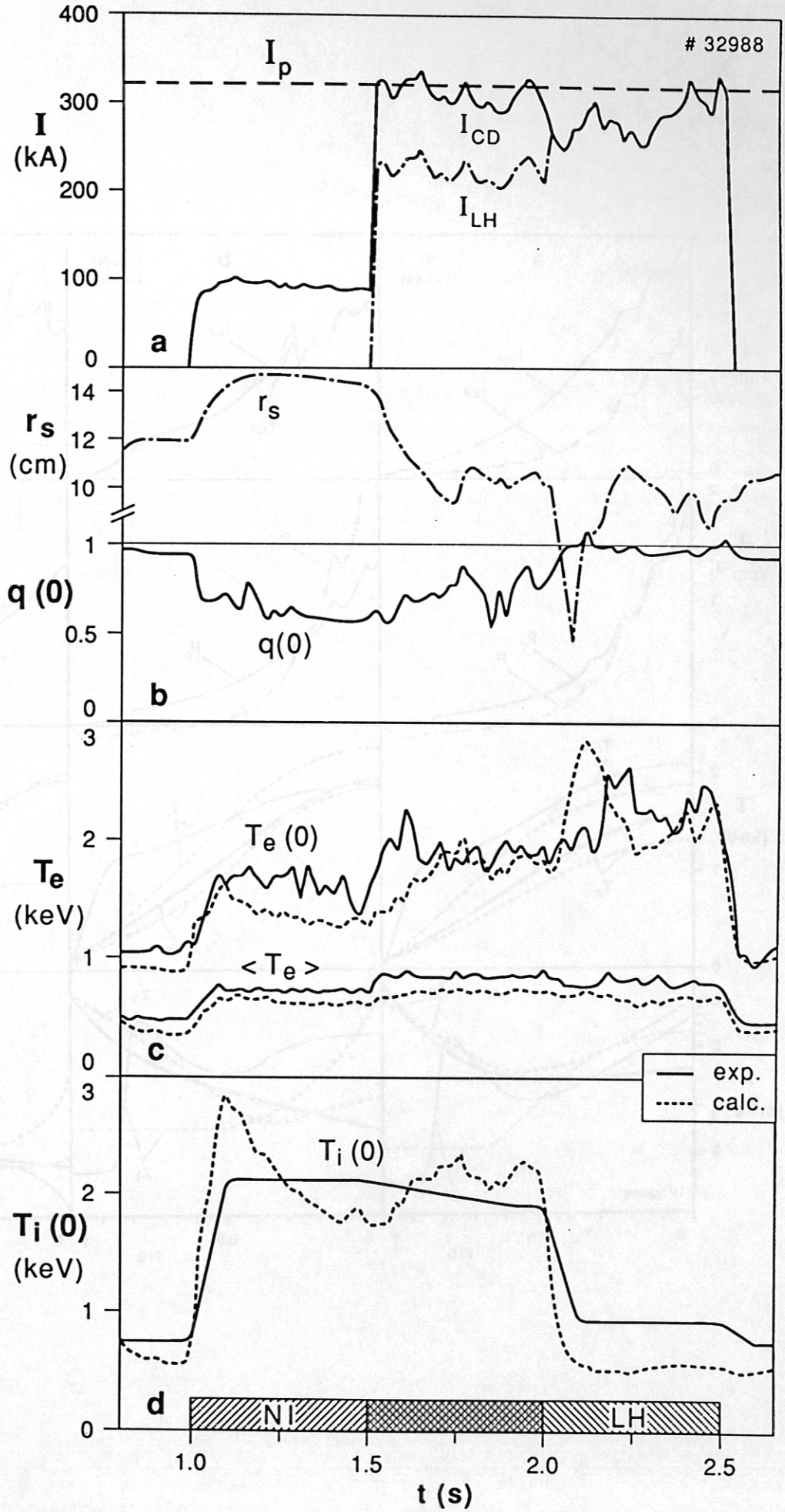
400
300
200
100
0
I
(kA)
32988
I_p
I_{CD}
I_{LH}
a
14
12
10
1
r_s
(cm)
r_s
q (0)
0.5
0
q(0)
b
3
2
1
0
T_e
(keV)
T_e (0)
< T_e >
c
exp.
calc.
3
2
1
0
T_i (0)
(keV)
T_i (0)
d
NI
LH
1.0
1.5
2.0
2.5
t (s)

Fig. 5

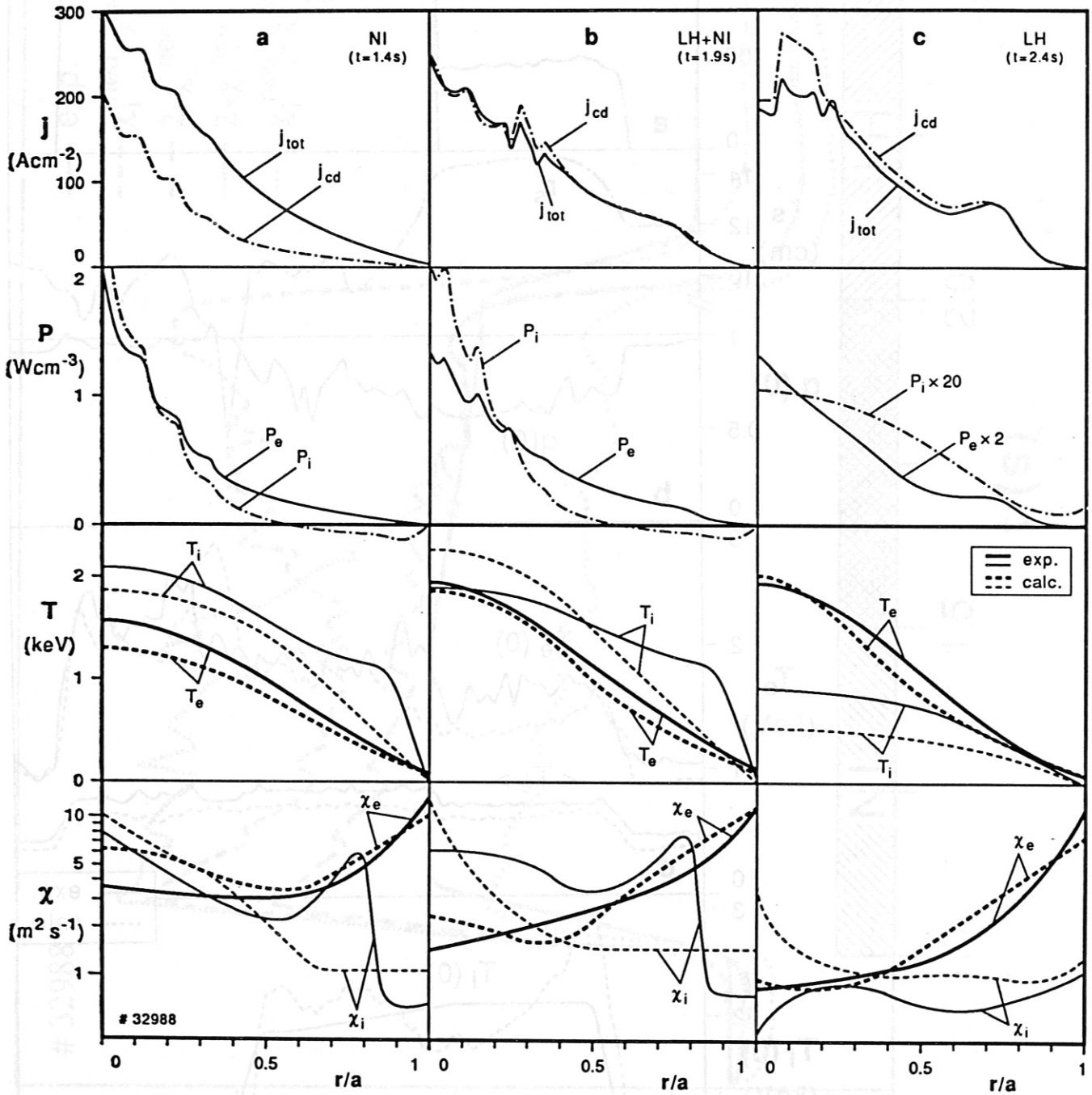
a
NI
(t=1.4s)
b
LH+NI
(t=1.9s)
c
LH
(t=2.4s)
j
(Acm-2)
300
200
100
0
jtot
jcd
P
(Wcm-3)
2
1
0
Pe
Pi
Pi × 20
Pe × 2
T
(keV)
Ti
Te
exp.
calc.
χ
(m2 s-1)
10
5
1
χe
χi
32988
0
0.5
1
r/a

Fig. 6